Materials and Design 196 (2020) 109186

Contents lists available at ScienceDirect

Materials and Design

journal homepage: www.elsevier.com/locate/matdes

Preparation of ZrB_2-ZrC-SiC-ZrO_2 nanopowders with in-situ grown homogeneously dispersed SiC nanowires

Changqing Liu [a,*], Luyue Zhang [a], Xiaoxiao Yuan [a], Hulin Liu [a], Chengxin Li [b,*], Xianghui Hou [c,*]

[a] School of Material Science and Engineering, Shaanxi Key Laboratory of Green Preparation and Functionalization for Inorganic Materials, Shaanxi University of Science &Technology, Xi'an, Shaanxi 710021, China
[b] State Key Laboratory for Mechanical Behavior of Materials, School of Materials Science and Engineering, Xi'an Jiaotong University, Xi'an, Shaanxi 710049, China
[c] Advanced Materials Research Group, The University of Nottingham, Nottingham NG7 2RD, UK

HIGHLIGHTS

- Homogeneously dispersed SiCnws in ZrB_2-ZrC-SiC-ZrO_2 nanopowders were in-situ synthesized through sol-gel method.
- The growth of SiCnws in the powder was rationally controlled by optimizing the precursor components.
- The content of ZrB_2 and ZrC in the powder was regulated by optimizing silicon content in the sol-precursor.

GRAPHICAL ABSTRACT

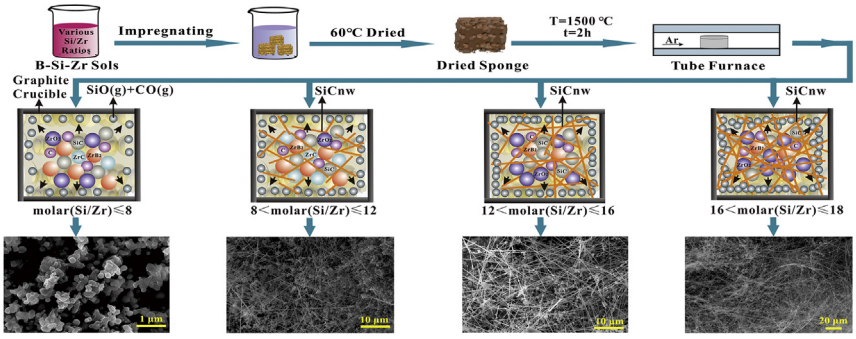

ARTICLE INFO

Article history:
Received 8 July 2020
Received in revised form 22 September 2020
Accepted 23 September 2020
Available online 25 September 2020

Keywords:
In-situ growth
SiC nanowires
ZrB_2-ZrC-SiC-ZrO_2
Nanopowder

ABSTRACT

To explore the application of SiC nanowires (SiCnws) in ZrB_2 based ceramic materials, a facile approach is reported to in situ synthesize homogeneously dispersed SiCnws in ZrB_2-ZrC-SiC-ZrO_2 nanopowders by pyrolyzing a B-Si-Zr containing sol precursor impregnated in polyurethane sponge. The sponge was used to provide porous skeletons for the growth of SiC nanowires and facilitate their uniform distribution in the powders. After heat-treatment of the precursor with a Si/Zr atomic ratio of 10 at 1500 °C for 2 h, ZrB_2-ZrC-SiC-ZrO_2 ceramic powders were obtained with an even and fine particle size of ~100 nm. The SiCnws were in a diameter of ~100 nm with a controllable length varying from tens to hundreds of microns by increasing the silicon content in the precursor. Moreover, the produced SiCnws were in high purity, and homogeneously dispersed in the hybrid nanopowders. The study can open up a feasible route to overcome the critical fabrication process in SiCnws reinforced ceramic matrix composites.

1. Introduction

The high melting points, high hardness, relatively low density, excellent chemical stability and good thermal stability of ZrB_2-ZrC-SiC composites make them potential candidates for high-temperature structural applications, such as thermal protection, engines, furnace element and hypersonic vehicles [1–7]. Although ZrB_2-ZrC-SiC composites have revealed greatly improved performance than the monophase or binary-phase systems [8–10], the critical problems such as the limit sinterability, inherent brittleness and poor oxidation resistance still restrict their engineering applications [11–14].

To improve the reliability and expand their application, toughening by reinforcements with large aspect ratio (e.g. short fibres, whiskers, etc) has been demonstrated effective in improving the fracture

* Corresponding authors.
E-mail addresses: liuchangqing@sust.edu.cn (C. Liu), licx@mail.xjtu.edu.cn (C. Li), Xianghui.Hou@nottingham.ac.uk (X. Hou).

https://doi.org/10.1016/j.matdes.2020.109186

performance of prepared composites [15–19]. Among various reinforcements, SiC nanowires (SiCnws) become the focus of attention due to their outstanding performance, such as larger aspect ratio, higher specific strength, and superior harsh environment resistance [20,21]. For example, the theoretical strength of SiCnws with a diameter of 100 nm (about 24 GPa) is much higher than that of SiC whisker (about 8GPa) [22]. The higher strength of SiCnws will make a greater contribution to the synthesized composites. However, the fabrication of SiCnws reinforced ceramic matrix composites remain challenging. Firstly, due to the high aspect ratio, SiCnws will easily get entangled together and are hard to be dispersed evenly in the composites. Therefore, it is necessary to explore a new approach to ensure the homogeneous distribution of SiCnws in the matrix, thus improving their reinforcement effect. Besides, the produced SiCnws are expected to have high crystallinity, with a sufficient amount. A meaningful attempt to overcome above issues is to in-situ synthesize evenly dispersed SiCnws in the ceramic matrix. Recently, Zhong et al. prepared ZrB_2-SiC powders with in-situ grown SiCnws through pyrolyzing ZrB_2 polymeric precursor by using Ni catalyst [23]. Whereas, besides the large amounts of impurities, the homogeneous dispersion of SiCnws cannot be achieved due to the inhomogeneous distribution of the catalyst. Chu et al. synthesized homogeneously dispersed SiCnws in silicon-based ceramic powders using Si, SiC and graphite as raw materials, in which the ceramic particles had an average size of ~7 μm [24]. Moreover, the free silicon was found to be crucial for the synthesis of SiCnws in this method, and residue silicon existing in the ceramic powders might deteriorate the properties of the final composites. Zheng et al. fabricated SiCnws by chemical vapour deposition (CVD) method using Si, phenolic resin, and ZrB_2 powder [25]. Besides the uneven particle size distribution, the obtained SiCnws contained a relatively high amount of SiO_2. In addition, this method was hard to obtain high productivity of powders, particularly for the multiphase powders. Zhang et al. fabricated SiCnws enhanced ZrB_2-based ceramic composites by in-situ growing SiCnws in the ZrB_2 powder through hot-pressing [26]. In this work, the in-situ growth of SiCnws was accomplished by a complicated procedure, including the preparation of ZrB_2-$ZrSi_2$ ceramic slurry, the construction of green body with enough handling strength, and the fabrication of a porous structure by pyrolyzing the green body. And also, SiCnws produced in this work were twisted with uneven diameters due to high density of defects. Therefore, it is essential to explore a reliable approach to prepared ZrB_2 based ceramic powders with in-situ grown SiCnws. As is well known, the amount, particular morphology and dimension of fiber reinforcements should be a critical factor for the microstructure and mechanical performance of ceramic composites. However, the controlled modulation of these factors for in-situ growing SiCnws has not been investigated yet.

Furthermore, considering the high sensitivity to defects of the ceramic composites, the introduction of component ZrO_2 has been proved effective in creating the needed structure and phases for defects self-healing during high-temperature application [27–29]. As reported, the addition of an appropriate amount of ZrO_2 contributes to higher composite compaction, decreased average particle size and an increased defects self-healing ability in ZrB_2-ZrC-SiC-ZrO_2 system [29]. Moreover, it is known that an enormous improvement in the mechanical properties can be achieved by reducing the component size in the composites towards nanoscales [30–32]. Therefore, to avoid the disadvantages on the mechanical properties of the ceramic parts caused by the grain growth during the traditional high-temperature fabrication process (e.g., hot pressing and spark plasma sintering), it would be favorable to prepare ceramic powders in nanoscales for high performance ceramic parts.

In the present work, a facile approach is reported to in situ synthesize SiCnws in ZrB_2-ZrC-SiC-ZrO_2 nanopowders through sol-gel process combined with a templating method without any catalyst. Good amount of SiCnws had been produced with tunable length and high purity, which were homogeneously dispersed in the hybrid nanopowders. The formation mechanism of the hybrid powders was investigated systematically. Moreover, the growth of SiCnws in the powder was rationally controlled by optimizing the precursor components. The successful preparation of hybrid powder provides an opportunity for further fabrication high-performance SiCnws reinforced ceramic matrix composites.

2. Experimental procedure

2.1. Materials

The following chemical reagents were supplied by Tianjin Komiou Chemical Reagent Co, Ltd., and used without further processed: Zirconium (IV) oxychloride octahydrate ($ZrOCl_2 \cdot 8H_2O$, AR), Hydrogen peroxide (H_2O_2, AR, concentration: 35%), Boric acid (H_3BO_3, AR), D-Glucose ($C_6H_{12}O_6$, AR), Tetraethyl orthosilicate (TEOS, AR), Polythylene glycol 600 (PEG-600, CP), and Ethanol (C_2H_6O, AR).

2.2. Sample preparation

In the typical synthetic procedure illustrated in Fig. 1, B-Si-Zr containing hybrid sol was prepared by mixing zirconium-containing sol (Zr-Sol), silicon-containing sol (Si-Sol), boron-containing sol (B-Sol) and a carbon source thoroughly. Zr-Sol was prepared by mixing 0.01 mol $ZrOCl_2 \cdot 8H_2O$, 20 mL ethanol and 2 mL H_2O_2, and stirred at room temperature for 1 h. B-Sol was prepared by dissolving 0.02 mol H_3BO_3, 0.05 mL PEG in 50 mL boiling ethanol. The carbon source was obtained by mixing 0.068 mol D-Glucose with 30 mL distilled water. A series of Si-Sol with various TEOS contents were obtained by dissolving a certain amount of TEOS in 20 mL ethanol. Specifically, the added amount of TEOS was 8, 12.5, 16.5, 20.5, 25, 29, 33 and 37.5 mL, respectively, based on the atomic ratio of silicon and zirconium, i.e., Si/Zr, which was 4, 6, 8, 10, 12, 14, 16 and 18, respectively. Finally, green bodies were prepared by impregnating polyurethane sponges (2 cm × 2 cm × 2 cm) in the above hybrid solution and fully dried at 60 °C. This impregnation and the dry process were repeated for three times. Finally, the obtained samples were taken out and put in a graphite crucible with a cover followed by heat-treating in a tube furnace under a pure argon atmosphere. For the sample with a Si/Zr atomic ratio of 12, the heat treatment was set to be 1300, 1400, 1500 and 1600 °C for 2 h, respectively, starting from room temperature at a heating rate of 5 °C/min. To further investigate the growth behavior of the hybrid powder, heat-treatment at 1500 °C was held for 1, 2, 3 and 4 h, respectively. Samples with various TEOS contents were heated at 1500 °C for 2 h, and the obtained hybrid powders were labelled as 4SZ, 6SZ, 8SZ, 10SZ, 12SZ, 14SZ, 16SZ and 18SZ, respectively.

During the process, carbon sponges were formed from the polyurethane sponges, used to suppress the growth and agglomeration of ceramic particles, as well as to provide porous skeletons for the growth of SiC nanowires. A high concentration of the reaction gases in the porous structure of the carbonized sponge could be achieved from the pyrolysis of the precursor, which benefits the growth and uniform distribution of SiC nanowires in the hybrid powders.

2.3. Characterization

Composition and structure of the hybrid gel were analysized by a Fourier transform infrared spectroscopy (FTIR, Vertex70, Bruker, Germany). Pyrolysis process of the prepared precursor was investigated by a thermogravimetric analyzer and differential scanning calorimetry (TG-DSC, STA449F3–1053-M, NETZSCH, Germany). Derivative thermogravimetry (DTG) curve was gained by differentiating the thermogravimetry (TG) curve. Composition of the ceramic powders was characterized by an X-ray powder diffractometer (XRD, D/max2200PC, Rigaku, Japan), with Cu Kα radiation in the range of

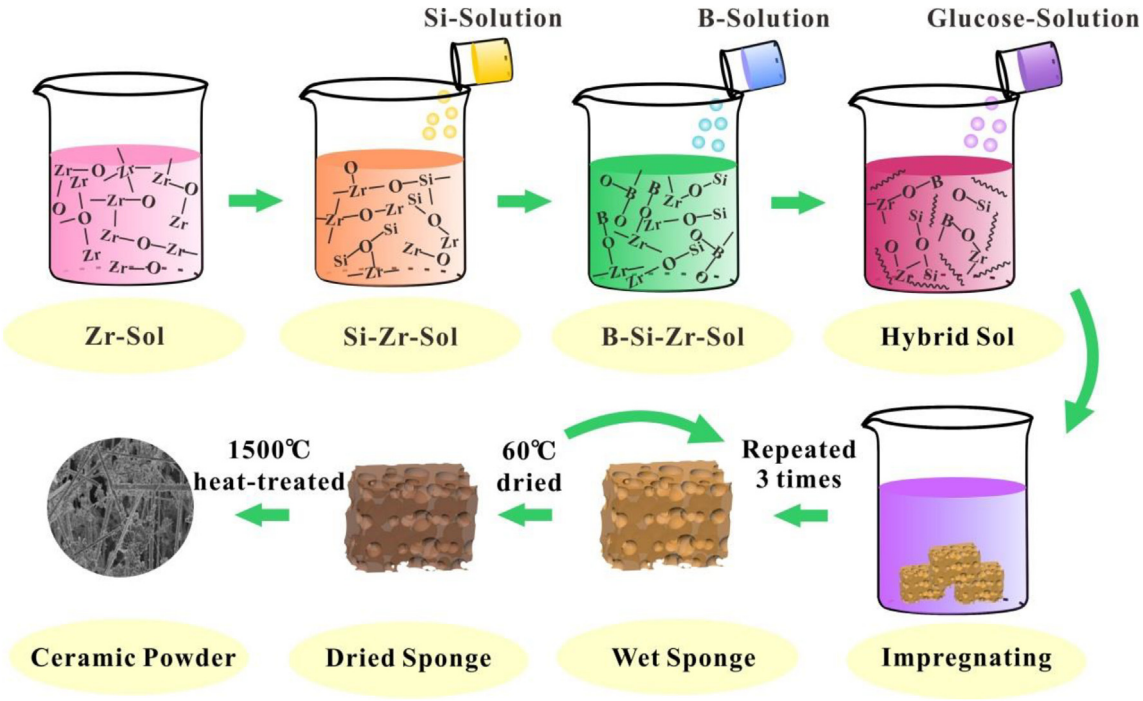

Fig. 1. Schematic diagram of the sample preparation.

10–70 degree. Morphologies of the ceramic powders were observed by scanning electron microscope (SEM, FEI Verios 460, USA). The microstructure of the products was also studied by an FEI Tecnai G2 F20 S-TWIN (high resolution) transmission electron microscope (TEM and HRTEM) equipped with an energy dispersive spectrometer (EDS) analysis.

In addition, the thermodynamic calculations of the reactions were conducted using Factsage thermochemical software. Gibbs free energies of the phases were obtained from the Fact compound databases.

3. Results and discussion

3.1. Microstructure of the prepared ZrB_2-ZrC-SiC(nw)-ZrO_2 hybrid powder

Fig. 2 shows the FTIR spectrum of the prepared precursor. In the spectrum, peaks at 1652 cm^{-1}, 1287 cm^{-1}, 1152 cm^{-1}, 1100 cm^{-1} and 680 cm^{-1} can be attributed to the absorption peaks of C═O, B—O, C—O, Si—O—Si and Zr—O bonds [33–36], respectively. The bands at 610 cm^{-1}, 540 cm^{-1} and 455 cm^{-1} correspond to the characteristic peaks of Si-O-B, Si-O-Zr and Zr-O-Zr bonds [35–37], respectively. These results indicate that boron, silicon, and zirconium elements have been incorporated into the precursor network, and the precursor presents in a highly hybrid structure.

Fig. 3 is the TG-DSC-DTG curves of the precursor under argon flow. As can be seen, the weight loss process mainly shows three stages. The first stage with nearly 50 wt% of mass loss happens below 670 °C with the maximum thermal decomposing temperature 361 °C and an endothermic peak around 222 °C in the DSC curve. This huge mass loss is mainly caused by the pyrolysis of the inorganic components and organic molecules, and the remove of residual solvents and small molecules. In the second stage, about 10 wt% of weight loss occurs during 670–1300 °C, which is caused by the further pyrolysis and carbonization of the intermediates generated in the first stage, and the formation and crystallization of oxides. For the third stage (temperature

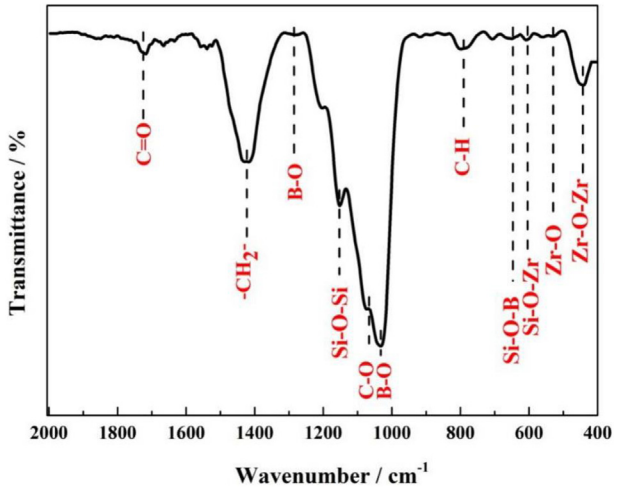

Fig. 2. FTIR spectrum of the prepared precursor. The sample ID is Si/Zr ratio = 12.

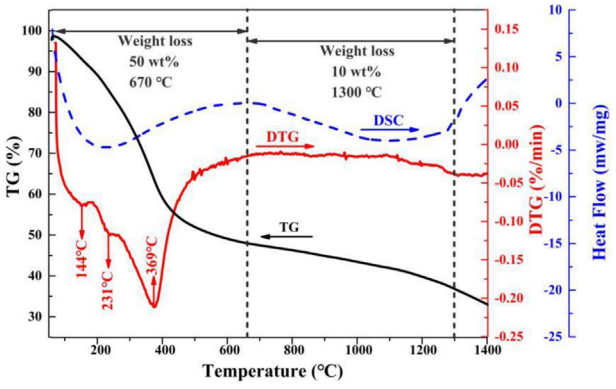

Fig. 3. TG-DSC-DTG curves of the precursor under argon flow. The sample ID is Si/Zr ratio = 12.

higher than 1300 °C), the TG curve shows an obvious weight loss accompanied with an endothermic peak (>1400 °C) in the DSC curve, which is probably resulted from the carbothermal conversion of oxides into carbides.

In this work, the prepared B-Si-Zr containing precursor was firstly introduced into the sponge, and then the green body was obtained after the wet sponge was fully dried. The green body was decomposed into ZrO_2, SiO_2, B_2O_3 and C after the pyrolysis process. And then, ZrB_2, ZrC and SiC nanostructures were produced by the following reduction reactions between the oxides and carbon:

$$ZrO_2\ (s) + B_2O_3\ (l) + 5C\ (s) = ZrB_2\ (s) + 5CO\ (g)$$
$$\Delta G^{\theta} = -845.35T + 1458474.8\ J \cdot mol^{-1} \quad (1)$$

$$SiO_2\ (s) + 3C\ (s) = SiC\ (s) + 2CO\ (g)$$
$$\Delta G^{\theta} = -339.70T + 606540.2\ J \cdot mol^{-1} \quad (2)$$

$$ZrO_2\ (s) + 3C\ (s) = ZrC\ (s) + 2CO\ (g)$$
$$\Delta G^{\theta} = -349.70T + 670443.5\ J \cdot mol^{-1} \quad (3)$$

Furthermore, due to the absence of metal catalyst, the growth of SiCnw can be explained by vapour solid (VS) growth mechanism [38,39]. The gaseous SiO and CO reactants can be produced by the following reactions [40–42]:

$$SiO_2\ (s) + C\ (s) = SiO\ (g) + CO\ (g) \quad (5)$$

$$SiO\ (g) + 3CO\ (g) = SiC\ (s) + 2CO_2\ (g) \quad (6)$$

CO_2 can be further reduced by free carbon atoms at high temperatures:

$$CO_2\ (g) + C\ (s) = 2CO\ (g) \quad (7)$$

If reaction (7) is thermodynamic equilibrium, reaction (8) can be obtained by combining reactions (6) and (7).

$$SiO\ (g) + 2C\ (s) = SiC\ (s) + CO\ (g) \quad (8)$$

Generally, reaction (8) is believed to be the key step for the synthesis of SiC nanowires. The Gibbs free energy ΔG for the growth of SiC nanowires is predicated by Eq. (9).

$$\Delta G = RT\ln\frac{P_{CO}}{K_{P(8)}P_{SiO}} \quad (9)$$

Correspondingly, the gas supersaturation (Σ) will be determined by the following formula:

$$\Sigma = \frac{P_{SiO}}{P_{CO}} \cdot K_{P(8)} \quad (10)$$

P_{CO} and P_{SiO} represent the partial pressure of CO and SiO vapour in the system, respectively. $K_{P(8)}$ refers to the equilibrium constant of reaction (8). R is the thermodynamic constant.

The morphology of SiC crystal is determined by the supersaturation of SiO and CO gases and the crystallization behavior of SiC. Usually, a relatively low gas supersaturation is essential to keep the growth of the nanowires. With a high gas supersaturation, the production of SiC particles will be favoured due to the formation of two-dimension SiC embryos [43].

The microstructure of the obtained ceramic powder was investigated by TEM and HRTEM, as shown in Fig. 4. TEM images indicate that the synthesized powder consists of fine particles with a diameter around 20–150 nm and nanowires. Fig. 4b suggests that the prepared nanowires were about 100 nm in diameter. EDS result indicates that the nanowires only contained Si and C elements (the insert of Fig. 4b), while the ceramic particles composed of Zr, B, C, O and Si elements (the insert of Fig. 4a). HRTEM image (Fig. 4c) and the SAED pattern (Fig. 4d) show that the SiCnw has a good single crystal structure. Furthermore, the crystal lattice fringe spacing was measured to be 0.254 nm, suggesting the SiCnw grows along the [111] direction [44,45]. Fig. 4e revealed that no catalyst droplets existed at the tips of the as-prepared SiC nanowire, indicating that the formation of SiC nanowire was controlled by vapour-solid mechanism [26,46]. Moreover, the inter-planner spacing of the particle on the nanowire is about 0.155 nm, which is ascribed to the (220) spacing of SiC [47], confirming the existence of SiC particles in the composite powder. The simultaneous existence of SiC particles and SiCnws may show a synergistic effect on the enhancement of mechanical performance of the fabricated composites [48].

Generally, a continuous generation of SiO and CO gases could induce the growth of SiC nanowires. Considering the local gas supersaturation will be affected by the insufficient or excess supplies, the separate partial pressures of SiO and CO vapours can be tailored by regulating the composition of reactants, the reaction temperature and the holding time, which are also bound to have impact on the growth of ZrB_2, ZrC and ZrO_2 nanoparticles.

3.2. Composition and morphology depending on heat-treatment temperature

Fig. 5 shows the XRD patterns of the hybrid powders obtained at different temperatures. After heat-treating at 1300 °C for 2 h in argon, only oxide phases, i.e. ZrO_2 and SiO_2, are detected. Due to the extremely low crystallization degree of the carbon phase and the easy vaporization of B_2O_3, no peaks of these two phases were detected in the XRD pattern. At 1400 °C, weak diffraction peaks of SiC appeared, with the oxide phases remaining as the main component. Further increasing the temperature to 1500 °C, ZrB_2 and SiC became the dominant phases, ZrC phase began to form, and there were residues of ZrO_2. After heat-treatment at 1600 °C, only ZrB_2, ZrC and SiC diffraction peaks in high intensity were detected, indicating the residue ZrO_2 was transformed into ZrC completely at this temperature. These results are in good consistent with the thermodynamic analysis shown in Fig. 6, which suggests the preferential formation of ZrB_2 and SiC (Fig. 6a) and higher stability of ZrB_2 (Fig. 6b).

Fig. 7 shows the morphologies of the ceramic powders obtained at various heat-treatment temperatures. The influence of temperature on the growth of SiCnw is proposed in Fig. 12a. For the sample obtained at 1300 °C (Fig. 7a), a bulk morphology with a flat surface and several dispersed short SiCnws are observed. Because at low temperature, reactions to produce gaseous SiO and CO did not occur. Due to the insufficient supply of gaseous SiO and CO, the growth of SiCnw cannot be retained, thus only very small amounts of short SiCnws are observed. In the case of 1400 °C (Fig. 7b), a higher amount of long SiCnw with relatively small diameter grew on the surface of the bulk material, the composition of which was mainly ZrO_2, SiO_2, carbon and SiC. Based on the result of XRD, low degree of the carbothermal reduction reaction happened to form SiC, accompanied by the generation of gaseous SiO and CO. Thus, SiCnws grew continuously under a low gas supersaturation at this temperature. At 1500 °C (Fig. 7c), the density of SiCnws abruptly increased. The diameter of SiCnws was increased to about 100 nm and their length was extended to tens of microns. Moreover, the obtained ZrC, ZrB_2 and ZrO_2 were fine and uniform particles with a size of about 100 nm, distributed around the SiCnw. At this temperature, the carbonization reactions to generate SiC, ZrC and ZrB_2 were enhanced, accompanied by the massive release of reactive gases (SiO, CO). Furthermore, the high temperature prompted the movement of the reaction gases, improving their collision frequency, and increasing the reactivity of the gas molecules. Therefore, with the increase of gas saturation, the growth of SiCnws was significantly improved. Further increasing the temperature to 1600 °C (Fig. 7d), agglomerated ceramic

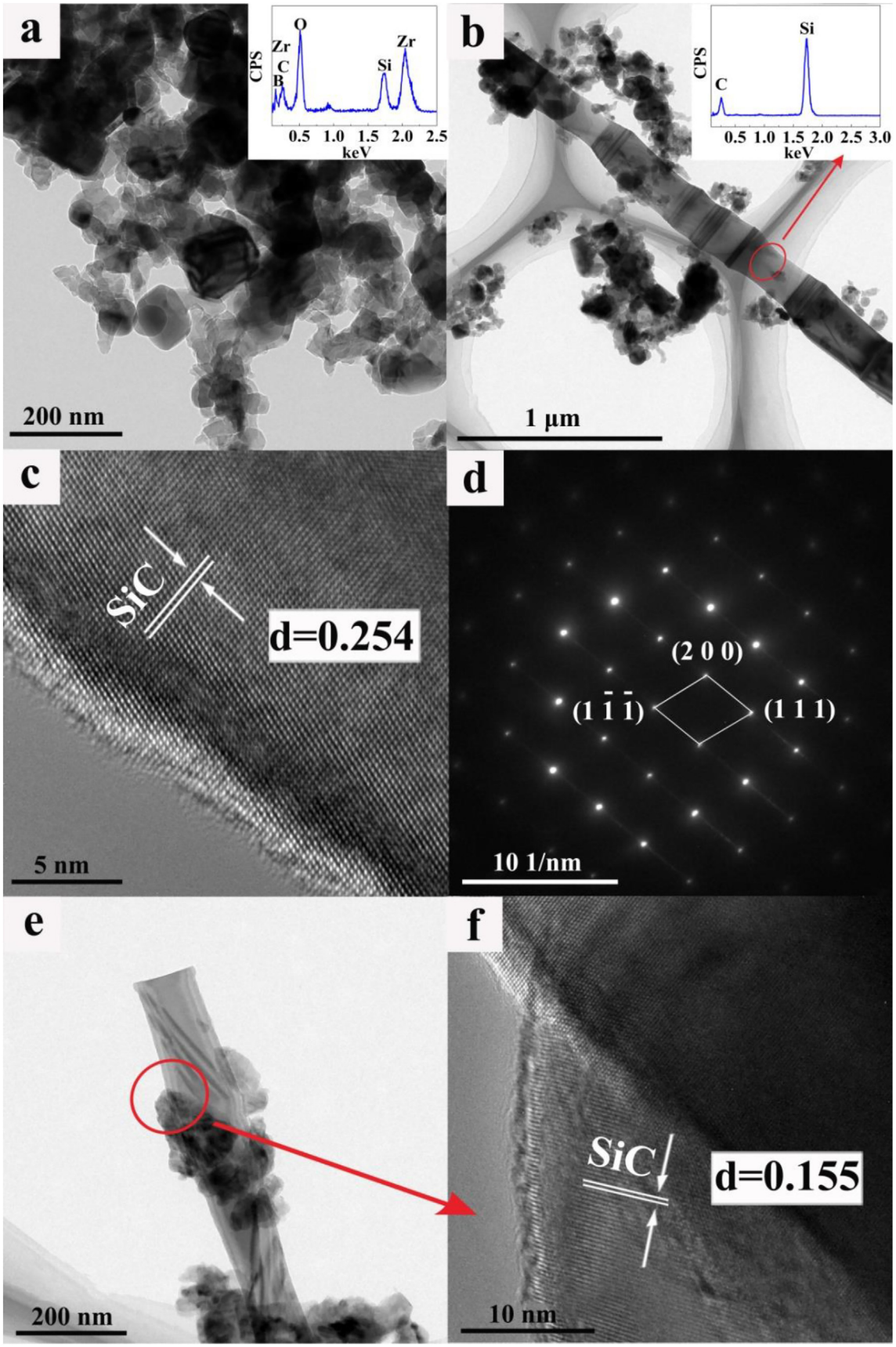

Fig. 4. (a) TEM images of ceramic particles and its corresponding EDS pattern(inset), (b) TEM images of ZrB_2-ZrC-SiC(nw)-ZrO_2 and the EDS analysis of SiC(nw) (inset), (c) HRTEM image of SiCnw and its corresponding SAED pattern (d), TEM (e) and HRTEM (f) images of the particle on the nanowire. The sample ID is Si/Zr ratio = 12, T = 1500 °C, t = 2 h.

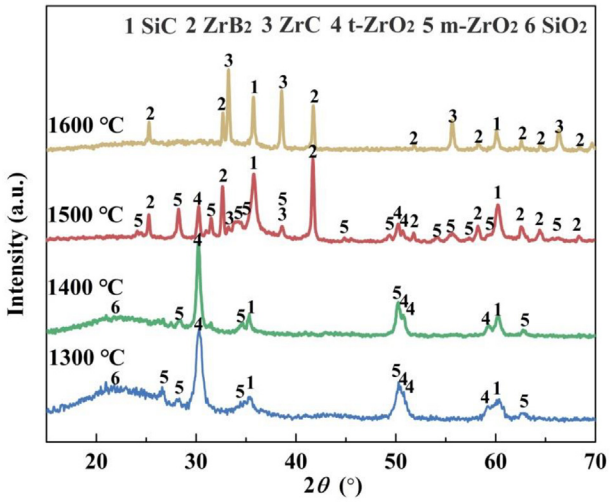

Fig. 5. XRD patterns of the samples with a Si/Zr ratio of 12 at various temperatures.

particles with uniformly dispersed short SiCnws can be observed. Gibbs free energy changed in the formation of ZrC, ZrB_2 and SiC through Eqs. (1)–(3) is negative at temperatures higher than 1600 °C. The massive generation of CO and SiO gaseous reactants during the carbonization reactions and the high temperature both contributed to the supersaturation level of the gaseous reactants (SiO, CO), hence large SiC crystal embryos were formed, which benefits the growth of SiC particles, instead of the one-dimensional nanowires.

Considering the above analysis, it can be deduced that ZrC, ZrB_2, SiC and ZrO_2 ceramic particles with the average particle size of 100 nm, and uniformly distributed SiC nanowires with the average diameter of 100 nm and the length beyond several tens of microns could be fabricated at 1500 °C. This observation indicates that the heat-treatment temperature of 1500 °C is optimum for the growth of SiCnw and the formation of fine ZrB_2-ZrC-SiC-ZrO_2 ceramic particles. So the temperature of 1500 °C was employed for all the rest studies.

3.3. Composition and morphology depending on holding times

Fig. 8 shows the XRD patterns of the powders after heat treatment at 1500 °C with various holding times. As observed, for a holding time of 1 h, sharp and strong diffraction peaks of ZrB_2 and SiC, as well as a minor phase of ZrO_2 (m,t) and SiO_2 were detected. As the holding time increased to 2 h, peaks ascribed to SiO_2 phase disappeared and low-intensity peaks ascribed to ZrC phase appeared. Meanwhile, the peak intensities of m-ZrO_2 and SiC increased. This result indicates the further development of these two phases from residue oxides. In the case of 3 h holding time, the peak intensities of m-ZrO_2, t-ZrO_2 and SiC further increased. Moreover, no peaks assigned to ZrC were detected, suggesting that there was none or very few ZrC in the materials fabricated at 1500 °C. Further increasing the holding time to 4 h, the content of ZrC, SiC and ZrB_2 showed no obvious changes, demonstrating that the carbothermal reduction reactions had completed at a holding time of 3 h. Moreover, it can be noted that the mass ratio of m-ZrO_2 to t-ZrO_2 was increased with the extension of holding time. From the above analysis, it is deduced that the extension of holding time contributes to transformation of t-ZrO_2 into m-ZrO_2 probably due to the higher stability of m-ZrO_2 at low temperatures.

Fig. 9 shows SEM images of the obtained ceramic powders at 1500 °C for various holding times. The influence of holding time on the growth of SiCnws is schematically presented in Fig. 12b. Different morphologies of SiCnws were observed in the samples. After heat-treating at 1500 °C for 1 h, granular particles and a few SiCnws with different lengths, diameters and morphologies were observed, which was caused by the large fluctuation of gas saturation due to insufficient supply of reaction gases. Extending the holding time from 1 h to 2 h, the residual SiO_2 continued to undergo carbonization to form SiC, resulting in an increase in the concentration of gaseous reactants (e.g. CO, SiO). Therefore, both the increased gas saturation and a longer growth time contributed to the intensive formation of SiCnws. Further prolonging the sintering time to 3 h, the growth of SiCnws continued under the continuous supplement of gases from the carbonization. Thus an obvious increase in the SiCnw length was obtained. When the holding time was 4 h, further growth of SiCnws in the ceramic powders was significantly reduced. From the microstructure of the SiCnws in Fig. 9d and 9d_1, it can be seen that the diameter of the SiCnws was finner, compared to that of 3 h holding time. Since no carbonization reactions occurred to produce reactant gases at this stage, the gaseous reactants were consumed to the growth of SiC crystals and the gases concentration in the system was diluted in Ar atmosphere. Therefore, the growth of SiCnws was restrained, due to the insufficient reaction gases for nanowires growth.

3.4. Composition and morphology depending on the Si/Zr ratio in the precursor

Fig. 10 shows the XRD patterns of the samples obtained from the precursors with various Si/Zr ratios heat-treated at 1500 °C for 2 h. Besides the continuously increased content of SiC, there are obvious changes in the peak intensities of key phases with the increasing of Si/Zr. When Si/Zr = 4, the main phases of m-ZrO_2, ZrB_2 and SiC, as

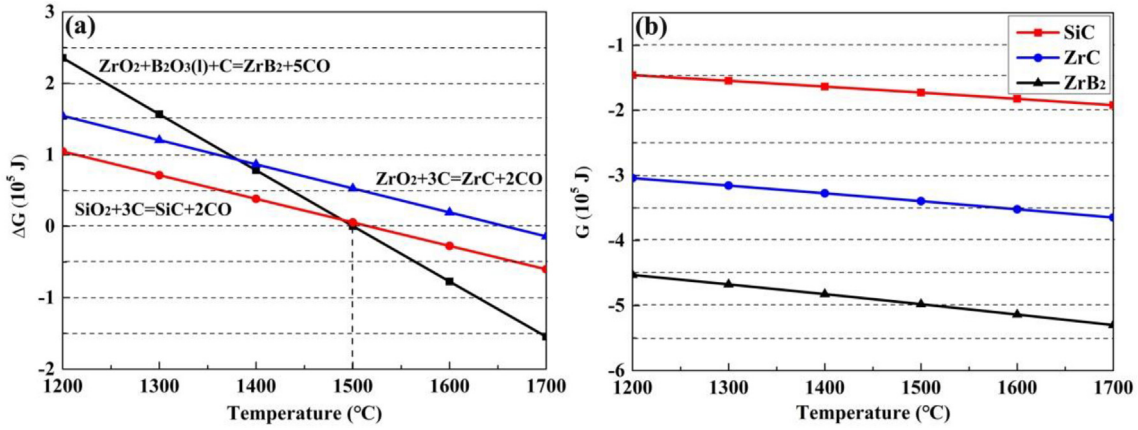

Fig. 6. (a) Thermodynamic calculations of reactions (11), (14) and (16) relative to temperature, (b) Gibbs energy of ZrC, ZrB_2 and SiC dependent on temperatures.

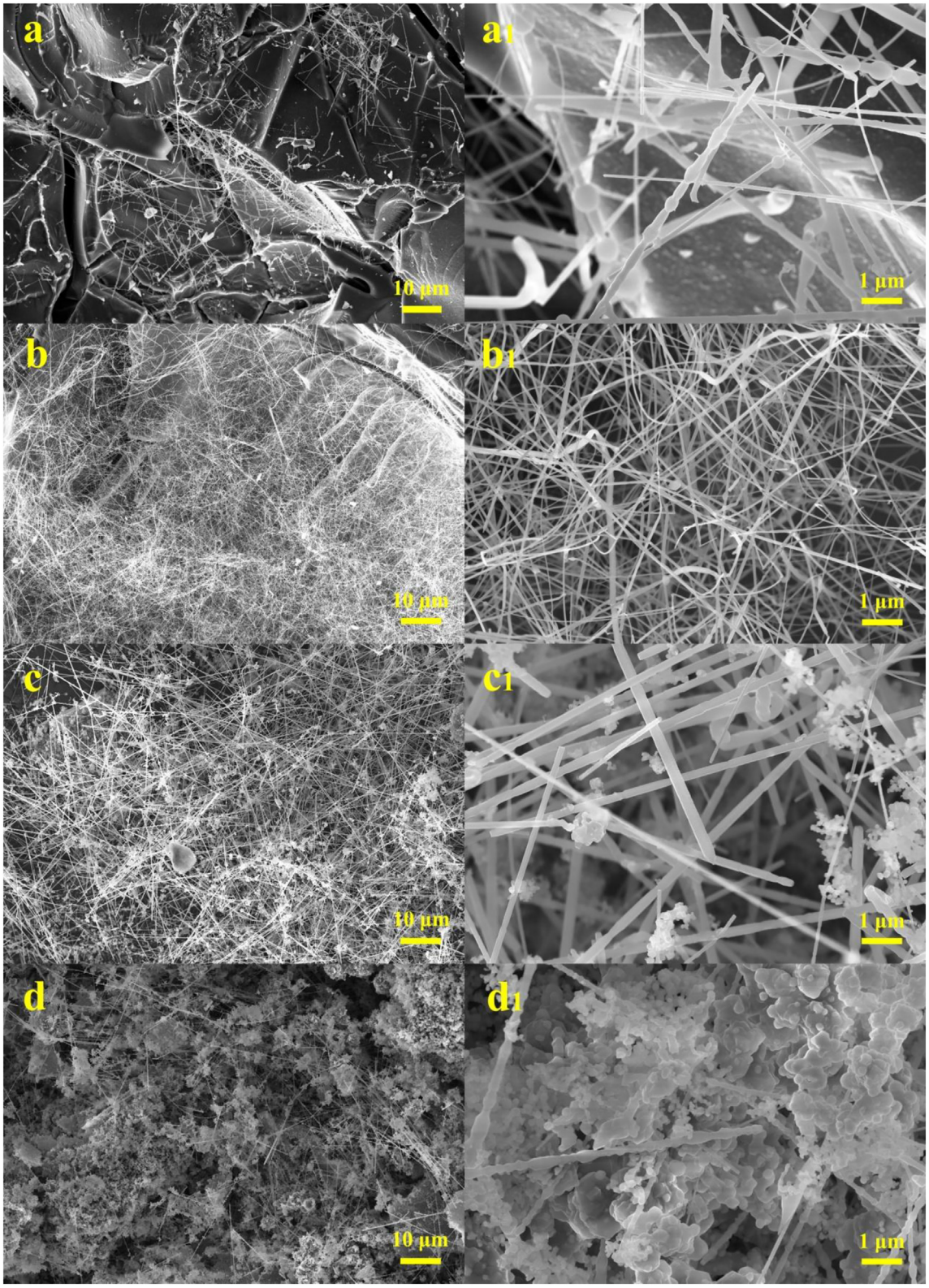

Fig. 7. SEM images of the samples with a Si/Zr ratio of 12 at various temperatures. (a) $T = 1300$ °C, (b) $T = 1400$ °C, (c) $T = 1500$ °C, (d) $T = 1600$ °C.

well as minor phases of t-ZrO_2 and ZrC were detected. By consistently increasing the Si/Zr ratio from 4 to 10, the content of ZrO_2 (m,t) decreased dramatically, while SiC, ZrC and ZrB_2 became the predominant phases. This result indicates that higher amount of silicon can benefit the full reaction between oxides and carbon, which may be due to the effects of grain refining as a result of the separation effect of silicon. At Si/Zr =12, low content of ZrC was detected. Moreover, as Si/Zr >12, dramatic decrease of both ZrB_2 and ZrC, as well as increase of t-ZrO_2 were detected. Ceramic powders with a composition of t-ZrO_2 and SiC as well as a minor phase of m-ZrO_2 and ZrB_2 were obtained. The relatively

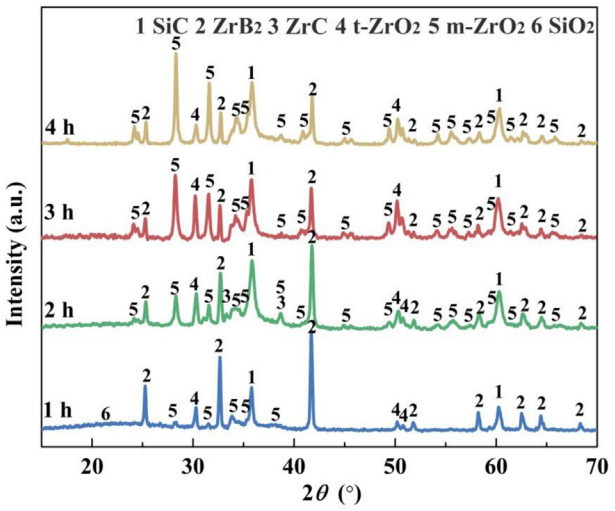

Fig. 8. XRD patterns of the samples with a Si/Zr ratio of 12 at various holding times at 1500 °C.

high content of t-ZrO_2 indicates that the high amount of silicon is beneficial to stabilize the phase of t-ZrO_2, which is the stable phase at high temperatures. The disappearance of ZrB_2 and ZrC may be attributed to the division between ZrO_2, carbon and B_2O_3 caused by the excessive silicon, and the evaporation of B_2O_3 at high temperatures.

The in-situ growth of SiCnws in the hybrid powders from the precursors with Si/Zr ratios varying from 4 to 18 are shown in Fig. S1–S3. Obviously, different morphologies were observed for the fabricated samples. The related schematic growth mechanisms of SiCnws was shown in Fig. 12c. The comparison results of the samples from the precursors with Si/Zr ratios of 4, 8, 12 and 18 are present in Fig. 11. Pure ceramic particles without nanowires were formed with a low silicon content of Si/Zr ≤8 (Fig. 11a and b), which was caused by the insufficient gas reactants for the growth of SiC nanowires. While a large number of SiCnws in different lengths grew with higher silicon contents were observed (Fig. 11c and d), together with uniformly distributed granular particles. When Si/Zr ratios were 10 and 12 (Fig. 11c), relatively short and straight nanowires, i.e. ~100 nm in diameter and ~tens of microns in length grew in both two samples, while relatively longer nanowires

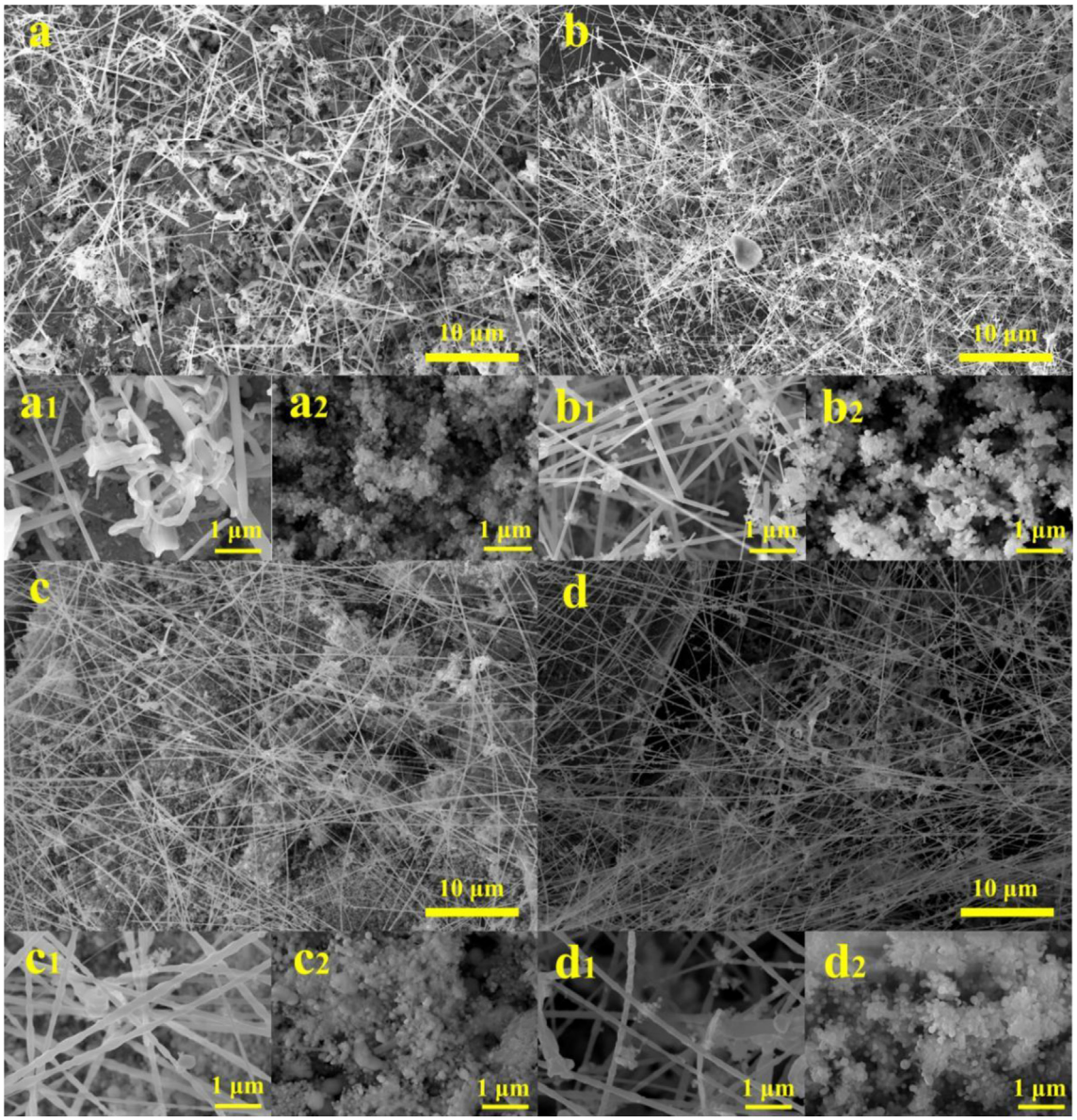

Fig. 9. SEM images of the samples with a Si/Zr ratio of 12 at various holding times at 1500 °C. (a, a_1, a_2) $t = 1$ h, (b, b_1, b_2) $t = 2$ h, (c, c_1, c_2) $t = 3$ h, (d, d_1, d_2) $t = 4$ h.

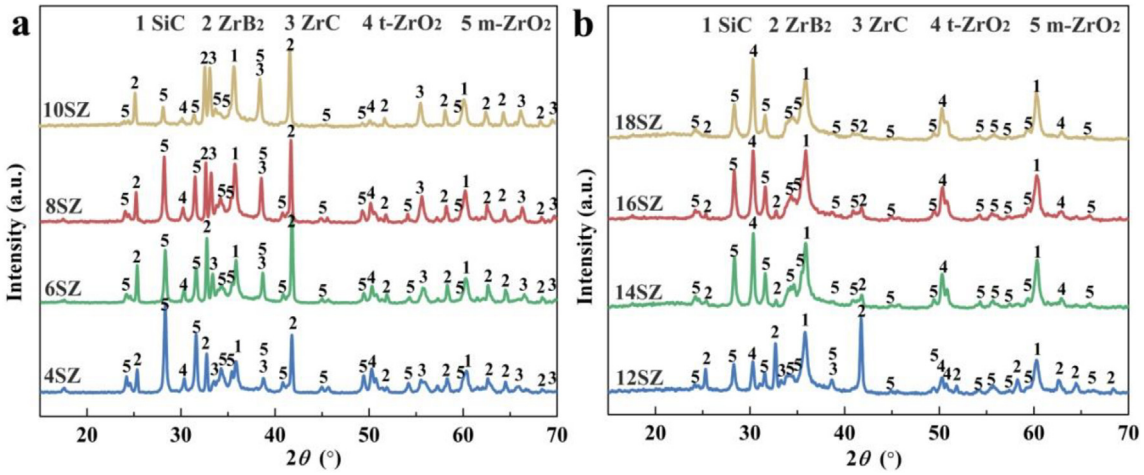

Fig. 10. XRD patterns of the samples from the precursors with various Si/Zr ratios.

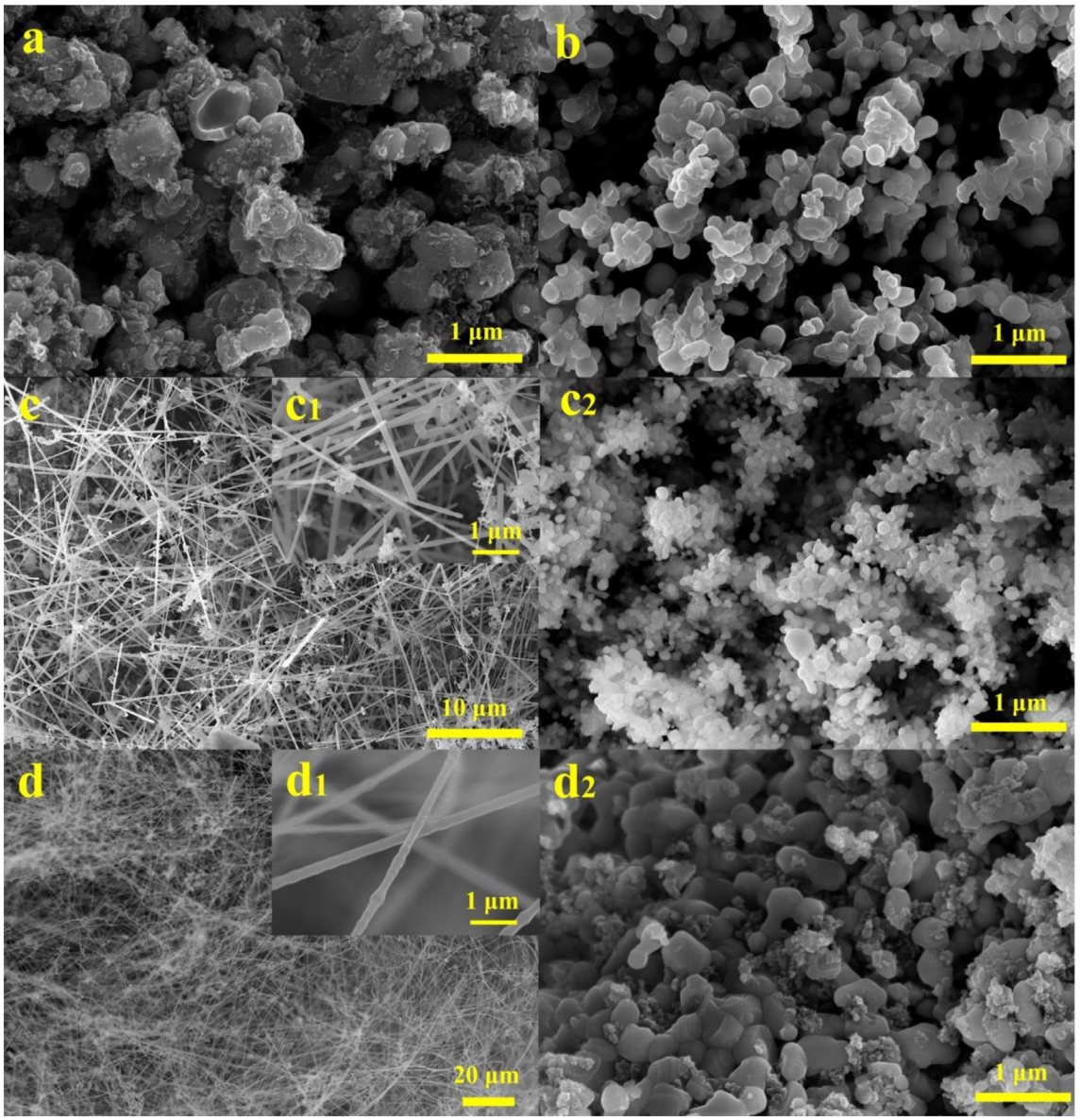

Fig. 11. SEM images of the samples from the precursors with various Si/Zr ratios. (a) Si/Zr =4, (b) Si/Zr =8, (c, c_1, c_2) Si/Zr =12, (d, d_1, d_2) Si/Zr =18.

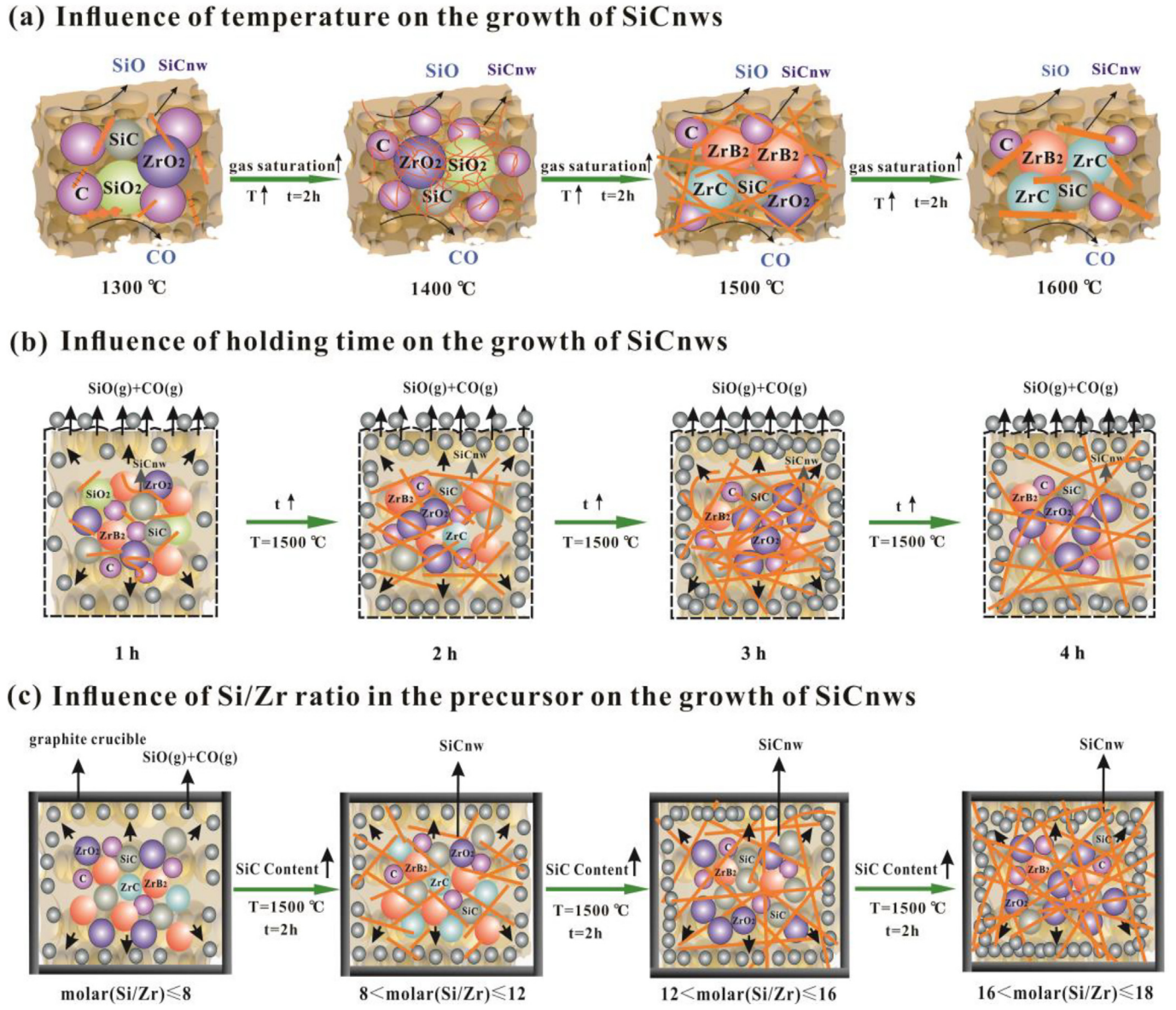

Fig. 12. Schematic showing the influence of (a) temperature, (b) holding time and (c) Si/Zr ratio in the precursor on the growth of SiCnws.

were observed for the sample with higher silicon content. For higher Si/Zr ratios of 14, 16 and 18 (Fig. 11d), significantly increase of the SiCnw length was achieved with the continuous supplement of SiO and CO gases. For sample with a Si/Zr ratio of 18, the length of SiCnws reaches up to hundreds of microns. Moreover, it can also be seen that the diameter of the nanowires retained to be around 100 nm in all the samples. These observations suggest that increasing silicon content in the precursor strongly affects the axial growth of nanowires, but has little effect on the radical growth.

Moreover, all the fabricated ceramic powders had even particle distribution. However, the average particle size decreased with the increase of silicon content. Specifically, by increasing the Si/Zr ratio from 4 to 8, the average particle size decreased from 500 nm (Fig. 11a) to less than 200 nm (Fig. 11b). Further increasing the Si/Zr ratio from 10 to 12, uniform dispersion of fine particles and nanowires were observed (Fig. 11c and 11c_2). However, for samples with Si/Zr ratios from 14 to 18, a particle coarsening tendency was found, especially, the sign for a certain degree of sintering was observed for the sample with the highest silicon content (Fig. 11d_2).

4. Conclusions

In conclusion, a facile approach of in-situ synthesizing homogeneously dispersed SiCnws in ZrB_2-ZrC-SiC-ZrO_2 nanopowders was demonstrated. Good amounts of homogeneously dispersed SiCnws were synthesized with high purity and a diameter of ~100 nm. The size of the produced ceramic particles was in nanoscale of ~100 nm. Furthermore, axial growth of the SiC nanowires was increased from tens of micron to hundreds of microns with the increasing the silicon content in the precursor. The in-situ growth of SiC nanowires in the nano-sized ZrB_2-ZrC-SiC-ZrO_2 powder and the controlled modulation of amount, morphology and dimension provide an opportunity for further fabrication of high-performance SiCnws reinforced ceramic matrix composites. Moreover, we demonstrate that increasing the silicon content in the precursor contributes to the refinement of the ceramic particles, prompting the formation of ZrC (Si/Zr ratio < 12), but the generation of both ZrB_2 and ZrC would be dramatically inhibited by further increasing the Si/Zr ratio in the precursor.

Data availability

The data is available upon request and please contact the corresponding author to access the data.

Declaration of Competing Interest

The authors declare that they have no known competing financial interests or personal relationships that could have appeared to influence the work reported in this paper.

Acknowledgements

This work was supported by the National Natural Science Foundation of China (grant numbers 51702194, 51702192); the Natural Science Foundation of Shaanxi Province (grant number 2018JQ5055); and the Research Startup Fund of Shaanxi University of Science and Technology (grant number 2016GBJ-09).

Appendix A. Supplementary data

Supplementary data to this article can be found online at https://doi.org/10.1016/j.matdes.2020.109186.

References

[1] A.L. Chamberlain, W.G. Fahrenholtz, G.E. Hilmas, D.T. Ellerby, High-strength zirconium diboride-based ceramics, J. Am. Ceram. Soc. 87 (6) (2010) 1170–1172.
[2] F.L. Li, Y.N. Cao, J.H. Liu, H.J. Zhang, S.W. Zhang, Oxidation resistance of ZrB_2 and ZrB_2-SiC ultrafine powders synthesized by a combined sol-gel and boro/carbothermal reduction method, Ceram. Int. 43 (2017) 7743–7750.
[3] R. Tu, B. Xiao, S. Zhang, Z. Deng, Q. Li, M. Yang, T. Goto, L. Zhang, H. Ohmori, Mechanical, electrical and thermal properties of ZrC-ZrB_2-SiC ternary eutectic composites prepared by arc melting, J. Eur. Ceram. Soc. 38 (2018) 3759–3766.
[4] M.Y. Zhang, K.Z. Li, X.H. Shi, W.L. Tan, Effects of SiC interphase on the mechanical and ablation properties of C/C-ZrC-ZrB_2-SiC composites prepared by precursor infiltration and pyrolysis, Mater. Design 122 (2017) 322–329.
[5] S.Q. Guo, Y. Kagawa, T. Nishimura, D. Chung, J.M. Yang, Mechanical and physical behavior of spark plasma sintered ZrC-ZrB_2-SiC composites, J. Eur. Ceram. Soc. 28 (2008) 1279–1285.
[6] F. Adibpura, S.A. Tayebifarda, M. Zakerib, M.S. Aslc, Spark plasma sintering of quadruplet ZrB_2-SiC-ZrC-C_f composites, Ceram. Int. 46 (2020) 156–164.
[7] J.Y. Zhao, L.V. Xuan, S.Y. Lai, L. Yang, W.J. Lei, X.G. Luan, R. Riedel, ZrC-ZrB_2-SiC ceramic nanocomposites derived from a novel single-source precursor with high ceramic yield, J. Adv. Ceram. 8 (1) (2019) 112–120.
[8] H.L. Liu, G.J. Zhang, J.-X. Liu, H. Wu, Synergetic roles of ZrC and SiC in ternary ZrB_2-SiC-ZrC ceramics, J. Eur. Ceram. Soc. 35 (2015) 4389–4397.
[9] H.B. Ma, G.J. Zhang, H.L. Liu, J.X. Liu, Y. Lu, F.F. Xu, Effect of WC or ZrC addition on thermal residual stresses in ZrB_2-SiC ceramics, Mater. Design 110 (2016) 340–345.
[10] S.Q. Guo, Y. Kagawa, T. Nishimura, D. Chung, J.M. Yang, Mechanical and physical behavior of spark plasma sintered ZrC-ZrB_2-SiC composites, J. Eur. Ceram. Soc. 28 (2008) 1279–1285.
[11] M.M. Oana, P. Neff, M. Valdez, A. Powell, M. Packard, L.S. Walker, E.L. Corral, Oxidation behavior of aerospace materials in high enthalpy flows using an oxyacetylene torch facility, J. Am. Ceram. Soc. 98 (2015) 1300–1307.
[12] C.Y. Tian, D. Gao, Y. Zhang, C.L. Xu, Y. Song, X.B. Shi, Oxidation behaviour of zirconium diboride-silicon carbide ceramic composites under low oxygen partial pressure, Corros. Sci. 53 (11) (2011) 3742–3746.
[13] F. Adibpur, S.A. Tayebifard, M. Zakeri, M.S. Asl, Co-reinforcing of ZrB_2-SiC ceramics with optimized ZrC to C_f ratio, Ceram. Int. 46 (2020) 22661–22673.
[14] W.G. Fahrenholtz, G.E. Hilmas, I.G. Talmy, J.A. Zaykoski, Refractory diborides of zirconium and hafnium, J. Am. Ceram. Soc. 90 (2007) 1347–1364.
[15] S. Guicciardi, L. Silvestroni, M. Nygren, D. Scitiw, Microstructure and toughening mechanisms in spark plasma-sintered ZrB_2 ceramics reinforced by SiC whiskers or SiC-chopped fibers, J. Am. Ceram. Soc. 93 (2010) 2384–2391.
[16] L. Silvestroni, D. Sciti, C. Melandri, S. Guicciardi, Toughened ZrB_2-based ceramics through SiC whisker or SiC chopped fiber additions, J. Eur. Ceram. Soc. 30 (11) (2010) 2155–2164.
[17] M.S. Asl, Y. Pazhouhanfar, A.S. Namini, S. Shaddel, M. Fattahi, M. Mohammadi, Role of graphite nano-flakes on the characteristics of ZrB_2-based composites reinforced with SiC whiskers, Diam. Relat. Mater. 105 (2020) 107786.
[18] C.L. Xia, M.S. Aslc, A.S. Namini, Z. Ahmadi, S.A. Delbari, Q.V. Le, M. Shokouhimehr, M. Mohammadi, Enhanced fracture toughness of ZrB_2-SiCw ceramics with graphene nanoplatelets, Ceram. Int. https://doi.org/10.1016/j.ceramint.2020.06.275.
[19] L. Zoli, A. Vinci, L. Silvestroni, D. Sciti, M. Reece, S. Grasso, Rapid spark plasma sintering to produce dense UHTCs reinforced with undamaged carbon fibres, Mater. Design 130 (2017) 1–7.
[20] R.H. Dong, W.S. Yang, P. Wu, M. Hussain, Z.H. Yu, L.T. Jiang, G.H. Wu, Effect of reinforcement shape on the stress-strain behavior of aluminum reinforced with SiC nanowire, Mater. Design 88 (2015) 1015–1020.
[21] W. Wang, Q. Fu, B. Tan, Effect of in-situ grown SiC nanowires on the mechanical properties of HfC-ZrB_2-SiC modified C/C composites, J. Alloys Compd. 726 (2017) 866–874.
[22] W. Yang, H. Araki, C. Tang, S. Thaveethavorn, A. Kohyama, H. Suzuki, T. Noda, Single-crystal SiC nanowires with a thin carbon coating for stronger and tougher ceramic composites, Adv. Mater. 17 (12) (2005) 1519–1523.
[23] Z.X. Zhong, L.W. Yan, L. Liu, B.S. Xu, Fabrication of modified ultrahigh-temperature ceramic hybrid powders using in situ grown SiC nanowires, Ceram. Int. 43 (2017) 3462–3464.
[24] Y.H. Chu, S.Y. Jing, J.K. Chen, In situ synthesis of homogeneously dispersed SiC nanowires in reaction sintered silicon-based ceramic powders, Ceram. Int. 44 (2018) 6681–6685.
[25] Q. Zhang, Z. Sun, X.G. Liu, J.J. Sun, R.H. Yu, X.H. Liu, Synthesis of SiC nanowires by a simple chemical vapour deposition route in the presence of ZrB_2, Ceram. Int. 46 (2020) 12249–12254.
[26] Z.F. Zhang, J.J. Sha, J.X. Dai, Y.F. Zu, Z.Z. Lv, Enhanced fracture properties of ZrB_2-based composites by in-situ grown SiC nanowires, Adv. Appl. Ceram. 118 (2019) 137–144.
[27] T.P. Nguyen, M.S. Aslc, S.A. Delbarid, A.S. Naminie, Q.V. Leg, M. Shokouhimehrd, M. Mohammadic, Electron microscopy investigation of spark plasma sintered ZrO_2 added ZrB_2-SiC composite, Ceram. Int. 46 (2020) 19646–19649.
[28] A.G. Burlachenko, Y.A. Mirovoy, S.P. Buyakova, E.S. Dedova, S.N. Kulkov, High-temperature laminated ceramic material HfC-ZrB_2-SiC-ZrO_2 for the development of the arctic and siberia, IOP Conf. Series: Mat. Sci. Eng. 696 (2019), 012008, .
[29] E.S. Dedova, A.G. Burlachenko, Y.A. Mirovoy, A.S. Buyakov, S.P. Buyakova, Self-healing in ZrB_2-ZrC-SiC-ZrO_2 ceramics, AIP Conf. Proc. 2167 (2019), 020067, .
[30] S.G. Chen, Y.Z. Gou, H. Wang, K. Jian, J. Wang, Preparation and characterization of high-temperature resistant ZrC-ZrB_2 nanocomposite ceramics derived from single-source precursor, Mater. Design 117 (2017) 257–264.
[31] E. Ionescu, H.J. Kleebe, R. Riedel, Silicon-containing polymer-derived ceramic nanocomposites (PDC-NCs): preparative approaches and properties, Chem. Soc. Rev. 41 (2012) 5032–5052.
[32] P. Hu, K. Gui, W. Hong, X. Zhang, S. Dong, High-performance ZrB_2-SiC-Cf composite prepared by low-temperature hot pressing using nanosized ZrB_2 powder, J. Eur. Ceram. Soc. 37 (6) (2017) 2317–2324.
[33] Y. Liu, R. Geng, Y. Cui, S. Peng, X. Chang, K. Han, M. Yu, A novel liquid hybrid precursor method via sol-gel for the preparation of ZrB_2 films, Mater. Design 128 (2017) 80–85.
[34] H. Moayyeri, R.M. Aghdam, R. Ghelich, F. Golestani-fard, In situ synthesis of ZrB_2-ZrC-SiC ultra-high-temperature nanocomposites by a sol-gel process, Adv. Appl. Ceram. 117 (2018) 189–195.
[35] A. Najafi, F.G. Fard, H.R. Rezaie, N. Ehsani, Synthesis and characterization of SiC nano powder with low residual carbon processed by sol-gel method, Powder Technol. 219 (2012) 202–210.
[36] K. Li, X. Zhou, Z. Zhao, C. Chen, C. Wang, B. Ren, L. Zhang, Synthesis of zirconium carbide whiskers by a combination of microwave hydrothermal and carbothermal reduction, J. Solid State Chem. 258 (2018) 383–390.
[37] H. Ji, M. Yang, M. Li, G. Ji, H. Fan, X. Sun, Low-temperature synthesis of ZrB_2 nanopowders using a sorbitol modified sol-gel processing route, Adv. Powder Technol. 25 (2014) 910–915.
[38] X.W. Du, X. Zhao, S.L. Jia, Y.W. Lu, J.J. Li, N.Q. Zhao, Direct synthesis of SiC nanowires by multiple reaction VS growth, Mater. Sci. Eng. B 136 (2007) 72–77.
[39] J.J. Liang, W.M. Guo, J.X. Liu, H. Qin, P.Z. Gao, H.N. Xiao, Synthesis of in-situ SiC nanowires by self-assembly nanoparticles on carbon fibers and their photoluminescence properties, J. Alloy Compd. 797 (2019) 101–109.
[40] X. Li, G.Q. Zhang, R. Tronstad, O. Ostrovski, Synthesis of SiC whiskers by VLS and VS process, Ceram. Int. 42 (2016) 5668–5676.
[41] H.J. Choi, J.G. Lee, Continuous synthesis of silicon carbide whiskers, J. Mater. Sci. 30 (1995) 1982–1986.
[42] L. Wang, H. Wada, L.F. Allard, Synthesis and characterization of SiC whiskers, J. Mater. Res. 7 (1992) 148–163.
[43] C. Lu, Mechanism of Chemical Vapor Deposition of Silicon Carbide From MTS/H_2 System, Ph.D. thesis Northwestern Polytechnical University, Xi'an, 2009.
[44] Z. Liu, Q.Q. Kong, C.M. Chen, Q. Zhang, L. Hu, X.M. Li, P.D. Han, R. Cai, From two-dimensional to one-dimensional structures: SiC nano-whiskers derived from graphene via a catalyst-free carbothermal reaction, RSC Adv. 5 (2015) 5946–5950.
[45] J. Dai, J. Sha, J. Shao, Y. Zu, M. Lei, S. Flauder, N. Langhof, W. Krenkel, In-situ growth of SiC nanostructures and their influence on anti-oxidation capability of C/SiC composites, Corros. Sci. 124 (2017) 71–79.
[46] J. Chen, W. Liu, T. Yang, B. Li, J. Su, X. Hou, K.-C. Chou, A facile synthesis of a three-dimensional flexible 3C-SiC sponge and its wettability, Cryst. Growth Des. 14 (2014) 4624–4630.
[47] R. Wu, Z. Yang, M. Fu, K. Zhou, In-situ growth of SiC nanowire arrays on carbon fibers and their microwave absorption properties, J. Alloy Compd. 687 (2016) 833–838.
[48] Y. Pazhouhanfar, A.S. Namini, S. Shaddel, Z. Ahmadi, M.S. Asl, Combined role of SiC particles and SiC whiskers on the characteristics of spark plasma sintered ZrB_2 ceramics, Ceram. Int. 46 (2020) 5773–5778.